Q-SHINE: a versatile sensor for glutamine measurement via ligand-induced dimerization

Moon-Hyeong Seo[1]*, Yun Lim[1], Ji Yul Kim[1], Youn Hee Jung[1], Jae Hoon Lee[2], Min Seok Baek[4], Je Hyeong Jung[2], Ho-Youn Kim[2], Wookbin Lee[1] and Keunwan Park[3]*

[1]Natural Product Research Center, [2]Smart Farm Research Center and [3]Natural Product Informatics Research Center, Korea Institute of Science and Technology, Gangneung, Republic of Korea,
[4]Department of Neurology, Wonju Severance Christian Hospital, Yonsei University Wonju College of Medicine, Wonju, Republic of Korea

*Corresponding authors

Moon-Hyeong Seo: e-mail: mhseo@kist.re.kr; phone: +82-33-650-3635

Keunwan Park: e-mail: keunwan@kist.re.kr; phone: +82-33-650-3663

Abstract

Studies on glutamine (Gln) metabolism have illuminated the vital role of Gln in cellular functions and its potential as a biomarker for disease detection. Despite the increasing interest in Gln metabolism, in-depth evaluations are challenging owing to limitations of conventional Gln-measuring methods. Thus, we developed a ligand-induced dimerization-based sensor for Gln, termed Q-SHINE, by splitting a glutamine binding protein into two separate domains. Q-SHINE enables highly accurate and convenient measurement of Gln concentration in bio-fluid samples, and the detection range is optimal for physiological Gln levels. Genetically encoded Q-SHINE sensors could also visualize intracellular Gln levels and quantify cytoplasmic and mitochondrial Gln change in living cells, which enabled detection of various cell responses to extracellular Gln supplement.

Keywords

Glutamine, Biosensor, Glutamine-binding protein, Periplasmic binding protein, Chemically induced dimerization

Abbreviations: QBP: glutamine-binding protein; LID: ligand-induced hetero-dimerization; PBP: periplasmic binding protein; BiFC: bimolecular fluorescence complementation; CBP: cysteine-binding protein; HBP: histidine-binding protein

1. Introduction

Glutamine (Gln) is a versatile amino acid that participates in the synthesis of nucleic acids, proteins, and anabolic processes to produce carbon and nitrogen. The optimal concentration of Gln is crucial in maintaining cellular integrity and function [1,2]. Previous studies have reported alterations in Gln levels in several diseases including cancer [2,3], diabetes[4,5], and neurodegeneration [6–8]. In particular, the consumption rate of Gln in cancer cells is significantly higher than that in normal cells, which indicates that Gln metabolism may be a key target for cancer treatment [2,3,9,10]. Therefore, supplementation or deprivation of Gln has been suggested to treat these diseases [2,7,11–14]. Previous studies have provided crucial insights into the significance of Gln levels in cellular functions and the potential application of Gln as a diagnostic biomarker of the relevant pathologies.

Measurement of Gln levels in physiological samples has previously been performed using analytic equipment (high-performance liquid chromatography [15–17] and amino acid analyzer [18]) or an enzyme-based colorimetric Gln assay [11,12]. However, the requirement of intricate preparation steps, such as cell lysis, deprotonation, and derivatization, hinders expanded use of these methods [19]. Furthermore, the accuracy of Gln assay kits are affected by underlying glutamate levels or other endogenous compounds interfering the enzymatic reactions. Alternatively, Gln concentration can be measured with spatiotemporal resolution in a genetically encoded manner via fluorescence-coupled sensors (based on FRET or circularly permuted fluorescent proteins) using a glutamine-binding protein (QBP) [20–23]. However, low dynamic range and frequent experimental errors limit their widespread adoption in the Gln metabolism research and diagnostic applications.

Here, we report a novel glutamine-sensing protein, Q-SHINE (Gln sensor via Split HINgE-motion binding protein), constructed by splitting a QBP via cleavage of two lobes. After divided, we confirmed the two independent domains of QBP reconstitute upon Gln binding. This ligand-induced hetero-dimerization (LID) system was subsequently coupled to a desired reporter, such as mCherry or NanoLuc, to transform the binding event into a detectable signal. Our LID-based Gln sensors, Q-SHINE_Red for fluorescence, and Q-SHINE_Luc for bioluminescence, provide a simplified protocol and higher specificity than conventional Gln assay kits, facilitating reagentless point-of-care diagnoses for diverse diseases related to Gln

62 metabolism. Genetically encodable Q-SHINE sensors effectively visualize intracellular Gln
63 levels, and further enable comparative quantification of cytoplasmic and mitochondrial Gln
64 changes in response to the environment of cancer and non-cancer cell lines.

2. Materials and Methods

2.1. Split design of PBPs

The domain movement of proteins was analyzed using DynDom [35]. In the case of QBP, two heterogeneous QBP conformers were compared (PDB ID: 1GGG and 1WDN). Results showed that QBP consists of two motional domains and exhibits an open-closed bending motion (rotation angle: 55.7 degree, and closure ratio: 99.8%). The residues situated in the hinge-bending region were 87–89 and 181–184 in the QBP (1WDN). Splitting the QBP at the two connecting strands generated two separate domains, where one domain (QBP_Lg) was fragmented into two segments. The discontinuous fragments were redesigned by modeling a new linker sequence, which connected the cleaved ends to generate a single polypeptide chain. Linker modeling was performed using RosettaRemodel with default options [36]; loop closure trials were attempted 10,000 times for loop lengths ranging from two to five. The designed loops were then filtered using LoopAnalyzerMover in RosettaScript [37]. The Rosetta total score, which summarizes loop quality, was used to select the final loop sequence that stabilized the fused domain. A shorter loop length was also prioritized to minimize flexibility. Structures of the designed domains were predicted using AlphaFold Colab [38].

2.2. Gene cloning for bacterial, mammalian, and plant cell expressions

Genes for the sensor components (QBP, mCherry, NanoBiT, and other PBPs with nucleotide sequences complementary to pET21a and Novagen at both ends) were synthesized by IDT gBlocks® Gene Fragments (Integrated DNA Technologies, Iowa, USA) and Gene Fragments (Twist Bioscience, South San Franscisco, USA). For bacterial expression, the pET21a plasmid was linearized through restriction with the NdeI and XhoI enzymes. The synthesized gene fragments were then cloned into the linear pET21a vector using the In-Fusion® HD Cloning Kit (Takara Bio, Kusatsu, Japan). For mammalian expression, the pcDNA3.1 (+) vector was linearized using PCR amplification. The split QBP and mCherry constructs were amplified, assembled, and cloned using the In-Fusion HD Cloning Kit. For plant cell expression, the whole expression cassette from the pcDNA plasmid was cloned into the pTALCOMT plasmid for Agrobacterium-mediated transformation [39].

94 **2.3. Protein expression and purification**

95 Plasmids containing the sensor constructs were transformed into *E. coli* BL21 (DE3) cells.
96 Protein expression was induced with 0.5 mM isopropyl b-D-1-thiogalactopyranoside at 18 °C.
97 Proteins were purified from the soluble cell lysate using His60 Ni Superflow Resin (Takara
98 Bio) and concentration was measured using NanoDrop. For analytical gel filtration
99 chromatography, the purified proteins from a Ni column were loaded onto a Superdex 75
100 Increase column equilibrated with 20 mM Tris-HCl (pH 8.0, 150 mM NaCl). Molecular mass
101 standards included conalbumin (75 kDa), ovalbumin (44 kDa), carbonic anhydrase (29 kDa),
102 and ribonuclease (13.7 kDa).

103

104 **2.4. *In vitro* BiFC**

105 Next, 5 μM of both sensor domains were mixed with different concentrations of Gln or other
106 amino acids in the Nunc Microwell 96-well Microplate (Thermo fisher, MA, US), and the
107 mixture was incubated in the dark for 1–5 h at 22 °C. Emission spectra of mCherry were read
108 in 1 nm increments from 600 to 620 nm using an Infinite M1000 (Tecan, Männedorf,
109 Switzerland) under 580 nm excitation.

110

111 **2.5. Mammalian cell culture**

112 Human embryonic kidney 293T (HEK293T) was purchased from the American Type Culture
113 Collection (ATCC). The cell line was tested for mycoplasma contamination and used only
114 within 30 passages. HEK293T was maintained in Dulbecco's Modified Eagle Medium
115 (DMEM; Gibco, Massachusetts, USA) supplemented with 10% (v/v) fetal bovine serum (FBS;
116 Gibco), 100 U/mL penicillin and 100 μg/mL streptomycin (P/S; Cytiva) at 37 °C in a
117 humidified 5% CO_2 incubator. HeLa cells (a gift from Dr. Lee, KIST, Korea) were maintained
118 in DMEM (Gibco) supplemented with 10% FBS (Gibco), and 1% PS at 37 °C.

119

120 **2.6. Bioluminescence measurement**

121 Next, 5 μM of two domains of Q-SHINE_Luc with 0–5 mM Gln for 10 min at 22 °C in the
122 dark. We also added 25 μL of the Nano-Glo Live Cell reagent included in the Nano-Glo Live
123 Cell Assay System (Promega) to each well and gently mixed for 10 s. Luminescence was
124 measured for a single time point using the GloMax Navigator System (Promega) and an
125 integration time of 1 s. For intracellular Gln quantification, cells were seeded at 1×10^4
126 cells/well in white/clear flat-bottom 96-well plates (Corning) and pCDNA plasmids harboruing
127 Q-SHINE_BL or mit-Q-SHINE_BL were transfected with 50 ng/well within 24 hours using
128 Lipofectamine 3000 reagent (Invitrogen) according to the manufacturer's instructions. For
129 glutamine starvation, cell culture medium was changed with glutamine-free DMEM (Gibco)
130 with 10% FBS before transfection and Opti-MEM medium (Gibco) was replaced with MEM
131 (Welgene). Glutamine added to final concentration at 0–2 mM after 16 h glutamine starvation.
132 Time-dependent bioluminescence was measured after glutamine addition using Nano-Glo®
133 Dual-Luciferase® reporter assay system (Promega). Cell culture plates were equilibrated at
134 22 °C. Next, 80 μL/well of ONE-Glo™ EX Reagent was added into 80 μL/well cell culture
135 medium and mixed on an orbital shaker (300 rpm) for 5 min at 22 °C. Then, firefly luciferase
136 activity was measured by a GloMax Navigator Microplate Luminometer (Promega) with 1 s
137 integration time. Subsequently, 80 μL NanoDLR™ Stop & Glo® Reagent was added to each
138 well, mixed for 10 min on an orbital shaker (600 rpm). NanoLuc activity also was measured
139 by a GloMax® Navigator Microplate Luminometer (Promega) with 1 s integration time. Data
140 were analyzed using Prism 9.0 (GraphPad Software).

141

142 **2.7. Measurement of Gln concentration in serum samples**

143 Female C57BL/6 mice, aged 6–12 weeks, were purchased from Orient-Bio (Seongnam, Korea).
144 The mice were cared for in accordance with institutional guidelines for experimental animals.
145 All experimental protocols were approved by the Animal Care and Use Committee of KIST
146 (Approval No. KIST-2021-09-104). To collect serum samples, blood was taken from the
147 abdominal caval vein and centrifuged at 300 ×*g* for 10 min at 4 °C after anesthesia was
148 administered and an abdominal incision was created. At least 200 μL serum was collected and
149 stored at -80 °C. For Gln measurement, 20 μL of serum samples from each mouse and different
150 concentrations of Gln solution were dissolved in distilled water. The samples were then mixed

151 with 5 μM of two domains of Q-SHINE_Red, followed by incubation in the dark and at 22 °C
152 for 5 h. The standard curve is fitted by nonlinear curve fitting method using the Hill1 function
153 in Origin 2020 (OriginLab Corporation, Northampton, USA), and the concentration of Gln in
154 serum samples was calculated using the 'Find X from Y' function based on the fitted graph.
155 For comparison, Gln concentration in mouse serum was simultaneously determined using the
156 EnzyChrom Glutamine Assay Kit (EGLN-100, BioAssay Systems, Hayward, CA, USA)
157 according to the manufacturer's protocol.

158

159 **2.8. Monitoring Gln changes in mammalian cells**

160 The mammalian expression vector was transiently transfected with Lipofectamine 3000
161 (Invitrogen, Thermo Fisher Scientific, Massachusetts, USA). For the intracellular bimolecular
162 fluorescence complementation (BiFC) experiments, HEK293T cells were seeded into 12-well
163 cell-culture treated plates (Thermo Fisher Scientific) and grown at 37 °C in 5% CO_2 overnight
164 in DMEM supplemented with 10% FBS and 1% P/S to 4–50% confluency. After the medium
165 was changed to DMEM (no Gln) supplemented with 10% FBS and 1% P/S to deprive the cells
166 of endogenous Gln, cells were transfected with plasmids containing Q-SHINE_FL or Q-
167 SHINE_BL proteins using Lipofectamine 3000. After 16 h of transfection, 0–2 mM of Gln
168 were added to the media for induction of Gln-dependent BiFC. Live cells were imaged with
169 the EVOS FL Cell Imaging System (Thermo Fisher Scientific) after the addition of Gln. To
170 obtain separate images of GFP and mCherry, two light cubes (470 nm excitation, 525 nm
171 emission; 530 nm excitation, and 593 nm emission) were used. Images from both channels
172 were overlaid to visualize overall fluorescence. Fluorescence intensities of mCherry and GFP
173 were quantified using Image J software (National Institutes of Health). The images were
174 segmented into each color in grayscale and the intensity of each fluorescence was measured on
175 a median scale after the ROI settings were established through threshold application.

176

177 **2.9. Transient expression and imaging of fluorescent proteins in tobacco leaves**

178 *Agrobacterium*-mediated transient expression analysis was performed as described by Lee et
179 al [40]. *Agrobacterium tumefaciens* LBA4404 cells carrying different sensor constructs were

180 adjusted to OD600 0.4 in resuspension solution (10 mM $MgCl_2$, 10 mM MES-KOH (pH 5.6),
181 100 µM acetosyringone) and infiltrated into leaves of 4 to 5-week-old *Nicotiana tabacum* cv.
182 Samsun. Plants were grown and incubated at 24/21 °C (day/night temperatures), for a 16 h
183 photoperiod, with 500 µmol/m^2/s light intensity and at 80 % relative humidity. At 5 days post-
184 infiltration, fluorescence intensities from the leaves were determined using an LSM5 Zeiss
185 confocal laser scanning microscope with the ZEN image analysis software (Carl Zeiss, Jena,
186 Germany). The excitation/emission spectra were 488/493–598 nm for GFP and 594/599–650
187 nm for mCherry.

188

189 **2.10. Statistical analysis**

190 Data from at least three independent experiments were expressed as the mean ± standard
191 deviation (SD). Statistical significance was determined using a one-way analysis of variance
192 followed by Tukey's multiple comparisons test using GraphPad Prism 9 (GraphPad Software).

193 **3. Results and Discussion**

194 **3.1. Split design of a Gln-binding protein**

195 QBP, a type II periplasmic binding protein (PBP), consists of two domains connected by a
196 hinge wherein a ligand binds to the region between two lobes. Ligand binding induces the
197 closing and twisting motions of the QBP that bring the lobes closer by hydrogen bonds between
198 the two domains and the ligand. Based on this structural feature, we converted *E.coli* QBP into
199 Gln-recognizing domains (Q-SHINE) that dimerize upon ligand binding (**Figure 1**). By
200 comparing the open and closed structures (PDB: 1GGG and 1WDN), the domain movement
201 of QBP through the hinge-bending motion was analyzed to estimate the cleavage sites that were
202 supposed to cause the least structural damage to the resulting split domains, and to ensure
203 minimal effect on ligand binding. Residues 87–89 and 181–184 (amino acid numbering in PDB
204 1WDN) were identified as hinge-bending regions and two domains were separated by the
205 deletion of Lys87-Ser88 and Ala182 (**Figure 2A**). Cutting two connecting strands of the QBP
206 results in noncontinuous fragment for a large domain (Lg; residues 1–86 and 183–226) and a
207 continuous fragment for a small domain (Sm; residues 89–181); thus, a linker was required for
208 the stable expression of the large domain. Of the three tested loops, a designed linker (TGNG)
209 that closed the gap between Tyr86 and Gln183 in QBP Lg displayed superior solubility when
210 expressed in *E.coli* (data not shown). AlphaFold showed the predicted structures of the two
211 divided domains, in which was insignificantly different from the global fold of the native QBP
212 (**Figure 2B**).

213 Each split QBP fragment, Lg and Sm, was subsequently recombined with split mCherry
214 fragments (MN159 & MC160),[24] which serve as reporter elements, resulting in the final
215 fusion construct, Q-SHINE_Red consisting of Split QBP_Lg-mCherry_C (LgC) and
216 mCherry_N – Split QBP_Sm (SmN) (**Figure 2C**). Gly-Ser linkers were used to link the split
217 QBP and mCherry fragments. Two domains of Q-SHINE_Red were analyzed first using gel
218 filtration chromatography. Both domains (LgC and SmN) moved faster than their expected size
219 (**Figure S1**), which might be because the nonnative structural configuration of the recombinant
220 fragments, which is elongated rather than spherical (**Figure 2C**) since the two independent
221 fragments are connected by a flexible linker. Interestingly, LgC was isolated as two separate
222 peaks (LgC_1 and LgC_2) while SmN was eluted as a single peak. However, when either

223 LgC_1 and LgC_2 was mixed with SmN in the presence of Gln, the signal-to-noise ratio (S/N;
224 mCherry fluorescence from the well with the ligand to the without ligand) of each pair
225 displayed insignificant differences. The complementation rate (the increase of fluorescence)
226 was faster when LgC_2 was used (data not shown). Although the underlying molecular
227 mechanism determining the difference of complementation efficiency remains elusive, LgC_2
228 was solely used in the subsequent experiments. Because split mCherry can associate without
229 being brought into close proximity by connected domains, the association rate of two domains
230 without Gln was examined by comparing Q-SHINE_Red and Q-SHINE_Red_ΔSm.
231 Fluorescence of Q-SHINE_Red_ΔSm is thought to be dependent on the self-assembly of split
232 mCherry domains merely because of QBP Sm deletion. Interestingly, Q-SHINE_Red exhibited
233 a significantly slower increase of fluorescence in the absence of Gln by the attenuated self-
234 assembly than that of Q-SHINE_Red_ΔSm (**Figure S2**). Fusion of the split QBP domain may
235 hinder the self-complementation of split mCherry fragments, which is beneficial for a higher
236 S/N ratio in measuring Gln concentration. Taken together, bimolecular fluorescence
237 complementation (BiFC) of the split mCherry domains of Q-SHINE_Red should provide a
238 qualitative and quantitative readout of the Gln-induced dimerization of split QBP domains,
239 thereby enabling the measurement of Gln concentration.

240 Next, we examined whether the split design could be adopted in other Type II PBPs with
241 structural similarity (*Campylobacter jejuni* cysteine-binding protein (CBP) [25] and *E. coli*
242 histidine-binding protein (HBP) [26]). However, a split CBP with an identical design strategy
243 showed limited dynamic range of Cys-dependent fluorescence and no His-dependent signal
244 from split HBPs (**Figure S3).** Given that the reported binding affinity of HBP is higher than
245 that of QBP and CBP (30, 300, and 100 nM, respectively), the imbalance in the binding mode
246 of His against two domains of HBP might be accountable for the poor ligand-induced
247 dimerization (**Table S2**). Although Q-SHINE uncovered the potential of a PBP family for a
248 novel ligand-responsive split system, the elaborate choice of a PBP scaffold and subsequent
249 design for split domains should be critical to the successful generation of a novel PBP-based
250 sensor.

251

252 **3.2. Gln measurement using Q-SHINE_Red**

253 To assess the ability of Q-SHINE_Red to detect Gln in solution, we combined equivalent
254 concentrations (5 μM) of Q-SHINE_Red proteins (LgC and SmN) with varying concentrations
255 of Gln. After incubating for a few hours, Gln-induced QBP dimerization was recognized by red
256 fluorescence in accordance with the proximity-induced complementation of mCherry (**Figure**
257 **3A**). While the signal contrast was maximized during the 3–6 h incubation period, the
258 sensitivity increased with a longer incubation time. In terms of analytical sensitivity, Q-
259 SHINE_Red could detect Gln concentrations as low as 1 μM. The emission peak was observed
260 at 610 nm, which is the reported value for the native mCherry protein (**Figure 3B**). The ligand
261 selectivity of Q-SHINE was further tested using structurally similar amino acids: glutamate,
262 asparagine and D-Gln. As shown in **Figure 3C**, Q-SHINE exhibited a highly specific reactivity
263 to Gln, clearly distinguishing it from other amino acids. Importantly, Q-SHINE_Red showed
264 notable sensitivity in the range of hundreds of μM to mM concentrations, demonstrating its
265 suitability for measuring physiological Gln levels which typically fall in the 200–1400 μM
266 range [12,19,22,27].

267 We sought to examine the performance of Q-SHINE by exchanging the reporting element with
268 a split luciferase. Unlike mCherry, NanoBiT is a reversible complementation system based on
269 enzymatic reactions that enable real-time kinetic analysis of live cells [28]. The split QBP and
270 NanoBiT fragments were recombined in a similar manner resulting in Q-SHINE_Luc (**Table**
271 **S2**). Similar to the results of Q-SHINE_Red, an increase in the bioluminescence was observed
272 in proportion to Gln concentration (**Figure 3D**). The sensitivity of the NanoBiT-based system
273 was commensurate with that of the Q-SHINE_Red because the sensing elements are essentially
274 identical in both systems. The Q-SHINE_Red showed a higher fold change in signals (i.e., high
275 signal-to-noise ratio) owing to cumulative fluorescence by irreversibly complemented mCherry,
276 while NanoBiT gave an immediate response in less than 10 min. This suggests that other split
277 reporter systems [29–31] such as β-lactamase, kinase, protease, biotin ligase, or Cas9, could be
278 readily combined with Q-SHINE for various applications.

279 We then investigated the performance of Q-SHINE_Red in quantifying Gln in a biological
280 sample. The each Q-SHINE domain was combined with 20 μL each four different mouse sera
281 as well as standard Gln solutions from 0 to 2 mM. Fluorescence intensities from the wells were
282 read by excitation at 587 nm and emission at 610 nm 5 h after incubation. The Gln

283 concentration of mouse sera was determined based on the standard curve obtained by plotting
284 the values from standard Gln solutions (**Figure S3**). Q-SHINE_Red provided data comparable
285 to a conventional and commercially available Gln colorimetric assay kit (**Figure 3E**).
286 Furthermore, intra-assay analysis verified the high repeatability and accuracy of Q-
287 SHINE_Red for the serum samples (**Figure 3F**). Cells, tissues, or clinical samples with high
288 glutamate or protein contents often result in high background signals in conventional
289 colorimetric Gln assays, which require additional pretreatment or background control.
290 Endogenous compounds may also interfere the enzymatic reactions. Given the limited
291 methodologies, Gln is one of the lesser-highlighted biomarkers despite the growing number of
292 reports demonstrating its relevance in multiple diseases, including cancer [2,11,27], diabetes
293 [4,5], and neurodegeneration [6–8]. The simple composition of Q-SHINE_Red, containing
294 only two protein domains, enables straightforward measurement without any pretreatment
295 process or expensive equipment. Q-SHINE_Red will therefore produce highly reliable and
296 accurate data in biological and biomedical research that utilizes conventional Gln assay kits.

297

298 **3.3. Monitoring Gln changes in living cells**

299 We investigated whether genetically encoded Q-SHINE could monitor intracellular Gln change.
300 For the equimolar expression of Q-SHINE fragments, a self-cleaving T2A peptide was inserted
301 between the two elements. GFP was also attached as an internal control to normalize mCherry
302 signal, resulting in Q-SHINE_FL (**Figure 4A**), which was expressed in Gln-deprived
303 HEK293T cells. It has been shown that the intracellular amino acid concentrations are largely
304 dependent on the amounts of amino acids in medium [32]. When different concentrations of
305 Gln were added to the medium, red fluorescence was detected from cells fluorescing GFP as a
306 control (**Figure 4B & Figure S4**). As expected, Q-SHINE-FL displayed red-to-green signal in
307 proportion to the Gln concentration and the incubation time. (**Figure 4C**). We also tested in
308 tobacco leaves to examine whether the biosensor could detect Gln in a different cellular
309 environment, and Q-SHINE-FL successfully visualized Gln in the plant cells (**Figure S5**).

310 For the quantitative analysis of intracellular Gln levels, we modified Q-SHINE_Luc into a
311 genetically encoded form of Q-SHINE_FL, resulting in Q-SHINE_BL (**Figure 4D**). Gln-
312 dependent bioluminescence ratio of NanoBiT to firefly luciferase (fLuc) from the live cells was

observed as expected (**Figure 4E**). We then expressed the biosensor in mitochondrial matrix by adding two tandem copies of the mitochondrial targeting signal from cytochrome c oxidase subunit VIII to the N-terminus of both Q-SHINE_BL fragments [32] (**Figure 4F**). We compared mit-Q-SHINE_BL and Q-SHINE_BL signals in both HEK293T and HeLa cell lines to explore the potential of our biosensor to specifically monitor and discriminate Gln levels in both cytosol and mitochondria. Indeed, homeostasis of Gln metabolism maintained by transport of Gln across plasma or mitochondria membrane, cytoplasmic glutamine synthesis, and mitochondrial glutaminolysis under various physiological conditions is vital for normal function and proliferation of cells [1]. Bioluminescence ratio was measured with the live cells after adding Gln to the medium. After different concentrations of Gln were added, time-dependent change of Gln levels either in cytosol or mitochondria was compared in both cells. As a result, Gln transport into the cytosol and/or de novo Gln synthesis in cytosol were faster and higher in HeLa, likely due to increased demand for Gln in cancer cells. In contrast, Gln levels in mitochondria were insignificantly different in two cell lines compared to those in cytosol (**Figure 4G**). Interestingly, Gln concentration in mitochondria was generally kept higher than that in cytosol of both cells. Taken together, Q-SHINE provides a simple and effective method of monitoring subcellular Gln levels. Further research utilizing the Q-SHINE system to address the underlying mechanisms how cells distinctly maintain subcellular Gln concentration should provide deeper insights into cellular Gln metabolism.

4. Conclusions

In this study, we developed an atypical Gln sensor system by split design of a QBP protein. Q-SHINE exhibits a strong signal-to-noise ratio and a detection range ideally suited to physiological Gln concentrations. The ligand-dependent dimerization of Q-SHINE enables direct measurement of Gln in bio-fluids with comparable sensitivity and higher specificity than a conventional Gln assay kit. Moreover, the performance of genetically encodable Q-SHINE for *in situ* Gln monitoring was demonstrated by comparing cytoplasmic and mitochondrial Gln changes in two distinct cell lines. Indeed, utilizing genetically encoded biosensors to monitor intracellular production or depletion of essential nutrients and metabolites has provided crucial insights by enabling non-invasive diagnosis [33], *in situ* detection of toxins [34], and development of biopharmaceuticals [22]. Collectively, our Gln sensor would facilitate in-depth studies on Gln metabolism and relevant diseases.

Declaration of competing interest

The authors declare that they have no known competing personal or financial interests that could influence the research reported in this paper.

Acknowledgments

We would like to thank Dr. Sungdo Ha for his valuable support in starting the project. We also thank Jisung Oh and Yebin Won for their help in the experiments.

Appendix A. Supplementary data

Supplementary data to this article can be found online.

Funding sources

This work was supported by an intramural grant from Korea Institute of Science and Technology; National Research Foundation of Korea (NRF) grant funded by the Korea government (MSIT) (2021R1C1C1003843).

359 **References**

360 [1] H.C. Yoo, Y.C. Yu, Y. Sung, J.M. Han, Glutamine reliance in cell metabolism, Exp.
361 Mol. Med. 52 (2020) 1496–1516. https://doi.org/10.1038/s12276-020-00504-8.

362 [2] C.T. Hensley, A.T. Wasti, R.J. DeBerardinis, Glutamine and cancer: Cell biology,
363 physiology, and clinical opportunities, J. Clin. Invest. 123 (2013) 3678–3684.
364 https://doi.org/10.1172/JCI69600.

365 [3] K.N. Rajagopalan, R.J. DeBerardinis, Role of glutamine in cancer: Therapeutic and
366 imaging implications, J. Nucl. Med. 52 (2011) 1005–1008.
367 https://doi.org/10.2967/jnumed.110.084244.

368 [4] N.F. Butte, H.W. Hsu, M. Thotathuchery, W.W. Wong, J. Khoury, P. Reeds, Protein
369 metabolism in insulin-treated gestational diabetes., Diabetes Care. 22 (1999) 806–811.
370 https://doi.org/10.2337/DIACARE.22.5.806.

371 [5] S.Y. Rhee, E.S. Jung, H.M. Park, S.J. Jeong, K. Kim, S. Chon, S.Y. Yu, J.T. Woo,
372 C.H. Lee, Plasma glutamine and glutamic acid are potential biomarkers for predicting
373 diabetic retinopathy, Metabolomics. 14 (2018) 1–10. https://doi.org/10.1007/s11306-
374 018-1383-3.

375 [6] H. Al-Otaish, L. Al-Ayadhi, G. Bjørklund, S. Chirumbolo, M.A. Urbina, A. El-Ansary,
376 Relationship between absolute and relative ratios of glutamate, glutamine and GABA
377 and severity of autism spectrum disorder, Metab. Brain Dis. 33 (2018) 843–854.
378 https://doi.org/10.1007/s11011-018-0186-6.

379 [7] J. Chen, Y. Chen, G. Vail, H. Chow, Y. Zhang, L. Louie, J. Li, R.P. Hart, M.R.
380 Plummer, K. Herrup, The impact of glutamine supplementation on the symptoms of
381 ataxia-telangiectasia: A preclinical assessment, Mol. Neurodegener. 11 (2016) 1–14.
382 https://doi.org/10.1186/s13024-016-0127-y.

383 [8] C. Madeira, C. Vargas-Lopes, C.O. Brandão, T. Reis, J. Laks, R. Panizzutti, S.T.
384 Ferreira, Elevated Glutamate and Glutamine Levels in the Cerebrospinal Fluid of
385 Patients With Probable Alzheimer's Disease and Depression, Front. Psychiatry. 9
386 (2018) 561. https://doi.org/10.3389/fpsyt.2018.00561.

387 [9] S. Tardito, A. Oudin, S.U. Ahmed, F. Fack, O. Keunen, L. Zheng, H. Miletic, P.Ø.
388 Sakariassen, A. Weinstock, A. Wagner, S.L. Lindsay, A.K. Hock, S.C. Barnett, E.
389 Ruppin, S. Harald MØrkve, M. Lund-Johansen, A.J. Chalmers, R. Bjerkvig, S.P.
390 Niclou, E. Gottlieb, Glutamine synthetase activity fuels nucleotide biosynthesis and
391 supports growth of glutamine-restricted glioblastoma, Nat. Cell Biol. 17 (2015) 1556–
392 1568. https://doi.org/10.1038/ncb3272.

393 [10] Y. Cormerais, P.A. Massard, M. Vucetic, S. Giuliano, E. Tambutté, J. Durivault, V.
394 Vial, H. Endou, M.F. Wempe, S.K. Parks, J. Pouyssegur, The glutamine transporter
395 ASCT2 (SLC1A5) promotes tumor growth independently of the amino acid transporter
396 LAT1 (SLC7A5), J. Biol. Chem. 293 (2018) 2877–2887.
397 https://doi.org/10.1074/jbc.RA117.001342.

398 [11] T.Q. Tran, E.A. Hanse, A.N. Habowski, H. Li, M.B. Ishak Gabra, Y. Yang, X.H.

399 Lowman, A.M. Ooi, S.Y. Liao, R.A. Edwards, M.L. Waterman, M. Kong, α-
400 Ketoglutarate attenuates Wnt signaling and drives differentiation in colorectal cancer,
401 Nat. Cancer. 1 (2020) 345–358. https://doi.org/10.1038/s43018-020-0035-5.

402 [12] M.B. Ishak Gabra, Y. Yang, H. Li, P. Senapati, E.A. Hanse, X.H. Lowman, T.Q. Tran,
403 L. Zhang, L.T. Doan, X. Xu, D.E. Schones, D.A. Fruman, M. Kong, Dietary glutamine
404 supplementation suppresses epigenetically-activated oncogenic pathways to inhibit
405 melanoma tumour growth, Nat. Commun. 11 (2020) 1–15.
406 https://doi.org/10.1038/s41467-020-17181-w.

407 [13] H.C. Yoo, S.J. Park, M. Nam, J. Kang, K. Kim, J.H. Yeo, J.K. Kim, Y. Heo, H.S. Lee,
408 M.Y. Lee, C.W. Lee, J.S. Kang, Y.H. Kim, J. Lee, J. Choi, G.S. Hwang, S. Bang, J.M.
409 Han, A Variant of SLC1A5 Is a Mitochondrial Glutamine Transporter for Metabolic
410 Reprogramming in Cancer Cells, Cell Metab. 31 (2020) 267-283.e12.
411 https://doi.org/10.1016/j.cmet.2019.11.020.

412 [14] M. Scalise, L. Pochini, M. Galluccio, C. Indiveri, Glutamine transport. From energy
413 supply to sensing and beyond, Biochim. Biophys. Acta - Bioenerg. 1857 (2016) 1147–
414 1157. https://doi.org/10.1016/j.bbabio.2016.03.006.

415 [15] S. Chen, S. Akter, K. Kuwahara, Y. Matsushita, T. Nakagawa, M. Konishi, T. Honda,
416 S. Yamamoto, T. Hayashi, M. Noda, T. Mizoue, Serum amino acid profiles and risk of
417 type 2 diabetes among Japanese adults in the Hitachi Health Study, Sci. Rep. 9 (2019)
418 1–9. https://doi.org/10.1038/s41598-019-43431-z.

419 [16] C.S. Kim, X. Ding, K. Allmeroth, L.C. Biggs, O.I. Kolenc, N. L'Hoest, C.A. Chacón-
420 Martínez, C. Edlich-Muth, P. Giavalisco, K.P. Quinn, M.S. Denzel, S.A. Eming, S.A.
421 Wickström, Glutamine Metabolism Controls Stem Cell Fate Reversibility and Long-
422 Term Maintenance in the Hair Follicle, Cell Metab. 32 (2020) 629-642.e8.
423 https://doi.org/10.1016/j.cmet.2020.08.011.

424 [17] J.K. Yan, K.J. Zhou, J.H. Huang, Q.Q. Wu, T. Zhang, C.C. Wang, W. Cai, Urinary
425 glutamine/glutamate ratio as a potential biomarker of pediatric chronic intestinal
426 pseudo-obstruction, Orphanet J. Rare Dis. 12 (2017) 1–4.
427 https://doi.org/10.1186/s13023-017-0615-3.

428 [18] A. Mustafa, S. Gupta, G.R. Hudes, B.L. Egleston, R.G. Uzzo, W.D. Kruger, Serum
429 amino acid levels as a biomarker for renal cell carcinoma, J. Urol. 186 (2011) 1206–
430 1212. https://doi.org/10.1016/J.JURO.2011.05.085.

431 [19] J.P. Hunt, R.J. Barnett, H. Robinson, M. Soltani, J.A.D. Nelson, B.C. Bundy, Rapid
432 sensing of clinically relevant glutamine concentrations in human serum with
433 metabolically engineered E. coli-based cell-free protein synthesis, J. Biotechnol. 325
434 (2021) 389–394. https://doi.org/10.1016/j.jbiotec.2020.09.011.

435 [20] J.D. Dattelbaum, J.R. Lakowicz, Optical determination of glutamine using a
436 genetically engineered protein, Anal. Biochem. 291 (2001) 89–95.
437 https://doi.org/10.1006/abio.2001.4998.

438 [21] H. Yang, M. Bogner, Y.-D. Stierhof, U. Ludewig, H+-Independent Glutamine

Transport in Plant Root Tips, PLoS One. 5 (2010) e8917. https://doi.org/10.1371/journal.pone.0008917.

[22] A. Behjousiar, C. Kontoravdi, K.M. Polizzi, In Situ Monitoring of Intracellular Glucose and Glutamine in CHO Cell Culture, PLoS One. 7 (2012) e34512. https://doi.org/10.1371/journal.pone.0034512.

[23] S. Takamatsu, J. Lee, R. Asano, W. Tsugawa, K. Ikebukuro, K. Sode, Continuous electrochemical monitoring of L-glutamine using redox-probe-modified L-glutamine-binding protein based on intermittent pulse amperometry, Sensors Actuators B Chem. 346 (2021) 130554. https://doi.org/10.1016/J.SNB.2021.130554.

[24] G.S. Filonov, K.D. Piatkevich, L.M. Ting, J. Zhang, K. Kim, V. V. Verkhusha, Bright and stable near-infrared fluorescent protein for in vivo imaging, Nat. Biotechnol. 29 (2011) 757–761. https://doi.org/10.1038/nbt.1918.

[25] A. Müller, G.H. Thomas, R. Horler, J.A. Brannigan, E. Blagova, V.M. Levdikov, M.J. Fogg, K.S. Wilson, A.J. Wilkinson, An ATP-binding cassette-type cysteine transporter in Campylobacter jejuni inferred from the structure of an extracytoplasmic solute receptor protein, Mol. Microbiol. 57 (2005) 143–155. https://doi.org/10.1111/J.1365-2958.2005.04691.X.

[26] N. Yao, S. Trakhanov, F.A. Quiocho, Refined 1.89-Å Structure of the Histidine-Binding Protein Complexed with Histidine and Its Relationship with Many Other Active Transport/Chemosensory Proteins, Biochemistry. 33 (1994) 4769–4779. https://doi.org/10.1021/bi00182a004.

[27] J.K. Byun, M. Park, S. Lee, J.W. Yun, J. Lee, J.S. Kim, S.J. Cho, H.J. Jeon, I.K. Lee, Y.K. Choi, K.G. Park, Inhibition of Glutamine Utilization Synergizes with Immune Checkpoint Inhibitor to Promote Antitumor Immunity, Mol. Cell. 80 (2020) 592-606.e8. https://doi.org/10.1016/j.molcel.2020.10.015.

[28] A.S. Dixon, M.K. Schwinn, M.P. Hall, K. Zimmerman, P. Otto, T.H. Lubben, B.L. Butler, B.F. Binkowski, T. MacHleidt, T.A. Kirkland, M.G. Wood, C.T. Eggers, L.P. Encell, K. V. Wood, NanoLuc Complementation Reporter Optimized for Accurate Measurement of Protein Interactions in Cells, ACS Chem. Biol. 11 (2016) 400–408. https://doi.org/10.1021/acschembio.5b00753.

[29] S.S. Shekhawat, I. Ghosh, Split-protein systems: Beyond binary protein-protein interactions, Curr. Opin. Chem. Biol. 15 (2011) 789–797. https://doi.org/10.1016/j.cbpa.2011.10.014.

[30] S.A. Lim, J.A. Wells, Split enzymes: Design principles and strategy, in: Methods Enzymol., Academic Press Inc., 2020: pp. 275–296. https://doi.org/10.1016/bs.mie.2020.05.001.

[31] M. Chen, C. Yan, Y. Ma, X.E. Zhang, A tandem near-infrared fluorescence complementation system with enhanced fluorescence for imaging protein–protein interactions in vivo, Biomaterials. 268 (2021) 120544. https://doi.org/10.1016/j.biomaterials.2020.120544.

[32] T. Yoshida, H. Nakajima, S. Takahashi, A. Kakizuka, H. Imamura, OLIVe: A Genetically Encoded Fluorescent Biosensor for Quantitative Imaging of Branched-Chain Amino Acid Levels inside Single Living Cells, ACS Sensors. 4 (2019) 3333–3342. https://doi.org/10.1021/ACSSENSORS.9B02067/ASSET/IMAGES/LARGE/SE9B02067_0001.JPEG.

[33] E.C. Greenwald, S. Mehta, J. Zhang, Genetically encoded fluorescent biosensors illuminate the spatiotemporal regulation of signaling networks, Chem. Rev. 118 (2018) 11707–11794. https://doi.org/10.1021/ACS.CHEMREV.8B00333/SUPPL_FILE/CR8B00333_SI_001.XLSX.

[34] M.J. Bick, P.J. Greisen, K.J. Morey, M.S. Antunes, D. La, B. Sankaran, L. Reymond, K. Johnsson, J.I. Medford, D. Baker, Computational design of environmental sensors for the potent opioid fentanyl, Elife. 6 (2017) e28909. https://doi.org/10.7554/eLife.28909.

[35] D. Taylor, G. Cawley, S. Hayward, Quantitative method for the assignment of hinge and shear mechanism in protein domain movements, Bioinformatics. 30 (2014) 3189–3196. https://doi.org/10.1093/BIOINFORMATICS/BTU506.

[36] P.S. Huang, Y.E.A. Ban, F. Richter, I. Andre, R. Vernon, W.R. Schief, D. Baker, RosettaRemodel: A Generalized Framework for Flexible Backbone Protein Design, PLoS One. 6 (2011) e24109. https://doi.org/10.1371/JOURNAL.PONE.0024109.

[37] S.J. Fleishman, A. Leaver-Fay, J.E. Corn, E.M. Strauch, S.D. Khare, N. Koga, J. Ashworth, P. Murphy, F. Richter, G. Lemmon, J. Meiler, D. Baker, RosettaScripts: A Scripting Language Interface to the Rosetta Macromolecular Modeling Suite, PLoS One. 6 (2011) e20161. https://doi.org/10.1371/JOURNAL.PONE.0020161.

[38] J. Jumper, R. Evans, A. Pritzel, T. Green, M. Figurnov, O. Ronneberger, K. Tunyasuvunakool, R. Bates, A. Žídek, A. Potapenko, A. Bridgland, C. Meyer, S.A.A. Kohl, A.J. Ballard, A. Cowie, B. Romera-Paredes, S. Nikolov, R. Jain, J. Adler, T. Back, S. Petersen, D. Reiman, E. Clancy, M. Zielinski, M. Steinegger, M. Pacholska, T. Berghammer, S. Bodenstein, D. Silver, O. Vinyals, A.W. Senior, K. Kavukcuoglu, P. Kohli, D. Hassabis, Highly accurate protein structure prediction with AlphaFold, Nature. 596 (2021) 583–589. https://doi.org/10.1038/s41586-021-03819-2.

[39] J.H. Jung, F. Altpeter, TALEN mediated targeted mutagenesis of the caffeic acid O-methyltransferase in highly polyploid sugarcane improves cell wall composition for production of bioethanol, Plant Mol. Biol. 92 (2016) 131–142. https://doi.org/10.1007/s11103-016-0499-y.

[40] J.H. Lee, H.J. Won, E.S. Oh, M.H. Oh, J.H. Jung, Golden Gate Cloning-Compatible DNA Replicon/2A-Mediated Polycistronic Vectors for Plants, Front. Plant Sci. 11 (2020) 1617. https://doi.org/10.3389/FPLS.2020.559365/BIBTEX.

Figure 1. Schematic of Q-SHINE design and Gln measurement. In step 1, based on the open and closed structure of glutamine-binding protein (QBP), hinge residues are selected by analysis of domain movement. In step 2, for the stable expression and proper function, suitable linker sequence was designed for the noncontinuous fragment. In step 3, the separate domains are fused with split reporter domains, such as split fluorescent protein and luciferase. In step 4, two components of the final sensor are mixed with samples or genetically expressed in cells. Resulting signals (fluorescence or bioluminescence) represent Gln level.

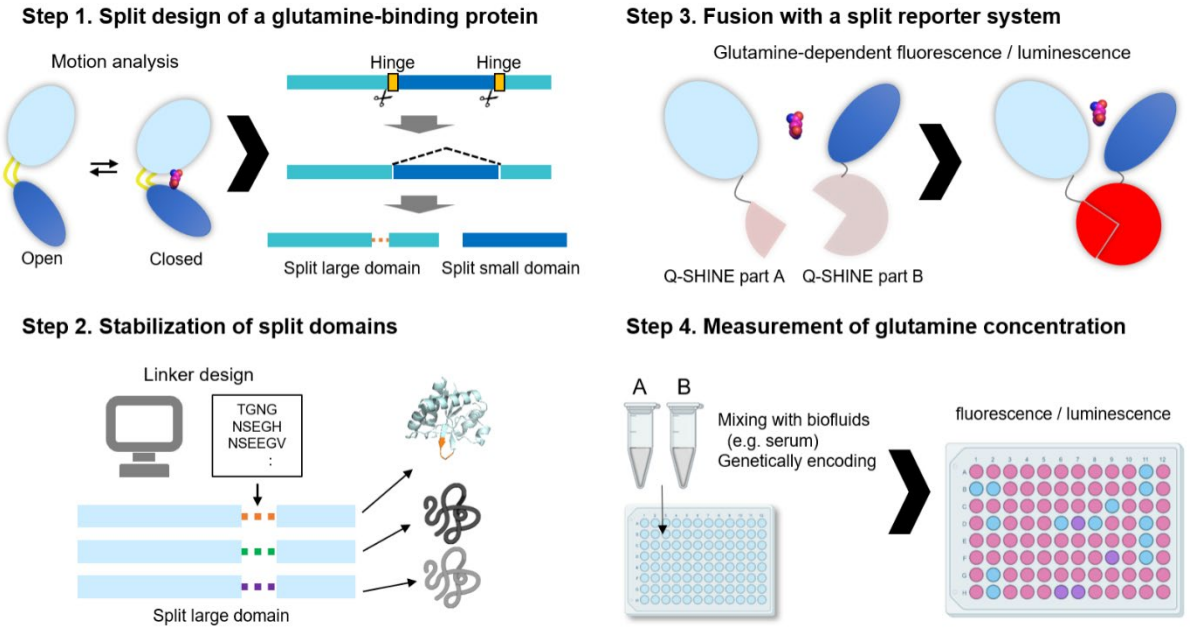

Figure 2. Design of split QBP and Q-SHINE_Red. (A) Based on the hinge-bending motion of *E. coli* QBP (PDB 1WDN), hinge residues (yellow) were selected for cleavage. One noncontinuous fragment was connected by the design of a new linker (red), resulting in two separate domains of QBP: QBP_Lg (light blue) and QBP_Sm (blue). (B) Structures of split domains were predicted by AlphaFold. When aligned with the holoprotein, two split domains showed the same global fold as in native QBP (RMSD 0.516 Å for QBP Lg, 0.418 Å QBP Sm). (C) Each split QBP domain was recombined with a split mCherry fragment for the construction of the complete Q-SHINE_Red system: Split QBP_Lg – mCherry_C (LgC) and mCherry_N – Split QBP_Sm (SmN). Gln-induced heterodimerization of QBP gives rise to red fluorescence by complementation of split mCherry fragments.

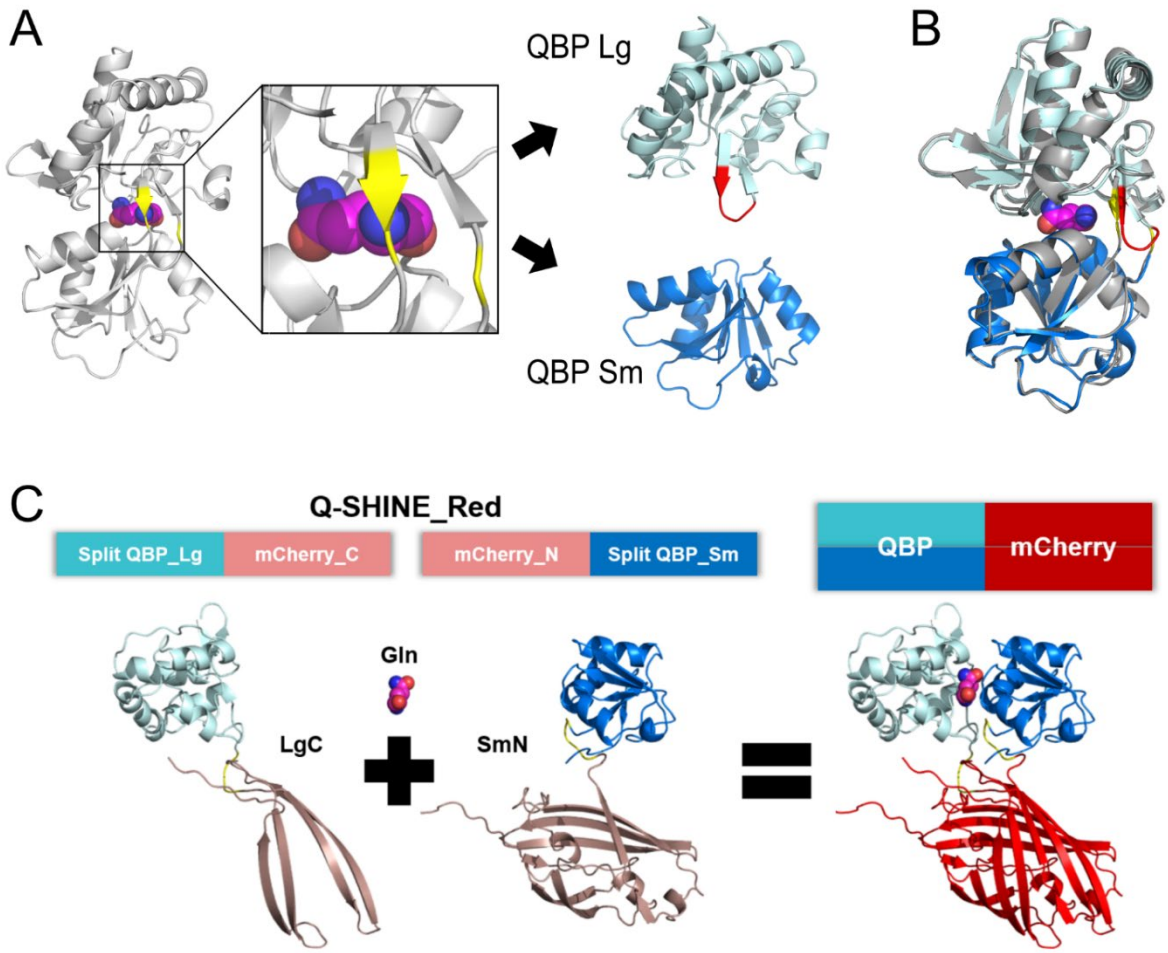

538 **Figure 3. Gln-measurement with Q-SHINE_Red and Q-SHINE_Luc.** (A) Gln-dependent
539 BiFC signal was measured with the marked concentration of Gln 2–94 h of incubation. Each
540 signal intensity was normalized to the well without Gln. (B) The representative emission
541 spectra changes by different Gln concentration. (C) Ligand selectivity of Q-SHINE_Red was
542 examined with other amino acids with similar structure. (D) Bioluminescence of Q-
543 SHINE_Luc increased depending on the Gln concentration. The x-axis represents the
544 corresponding Gln concentration in the reaction mixture. Data were normalized to the signal
545 from the wells no amino acid added. Error bars represent the s.d. in triplicate experiments. (E)
546 Comparison of Q-SHINE_Red against a commercially available Gln assay kit in measuring
547 Gln concentration of mouse serum. Pearson's correlation coefficient, $R^2 = 0.9938$, $P = 0.0062$.
548 (F) Intra-assay variability of Q-SHINE_Red for measuring Gln concentration in mouse serum.

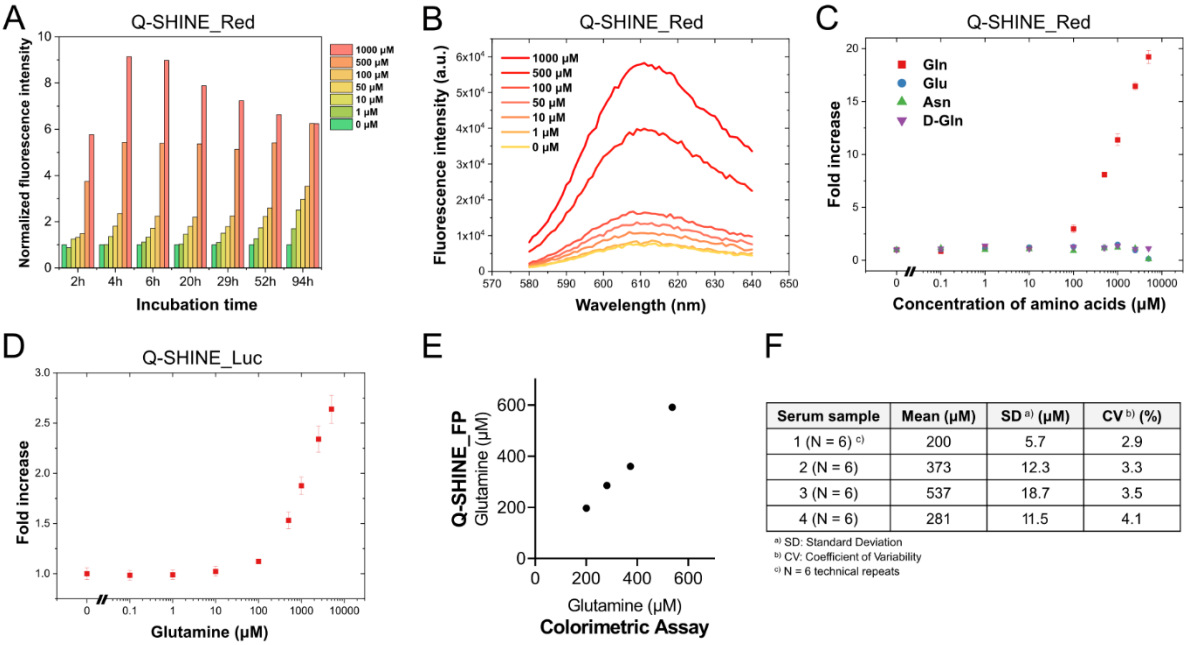

Serum sample	Mean (μM)	SD [a] (μM)	CV [b] (%)
1 (N = 6) [c]	200	5.7	2.9
2 (N = 6)	373	12.3	3.3
3 (N = 6)	537	18.7	3.5
4 (N = 6)	281	11.5	4.1

[a] SD: Standard Deviation
[b] CV: Coefficient of Variability
[c] N = 6 technical repeats

549
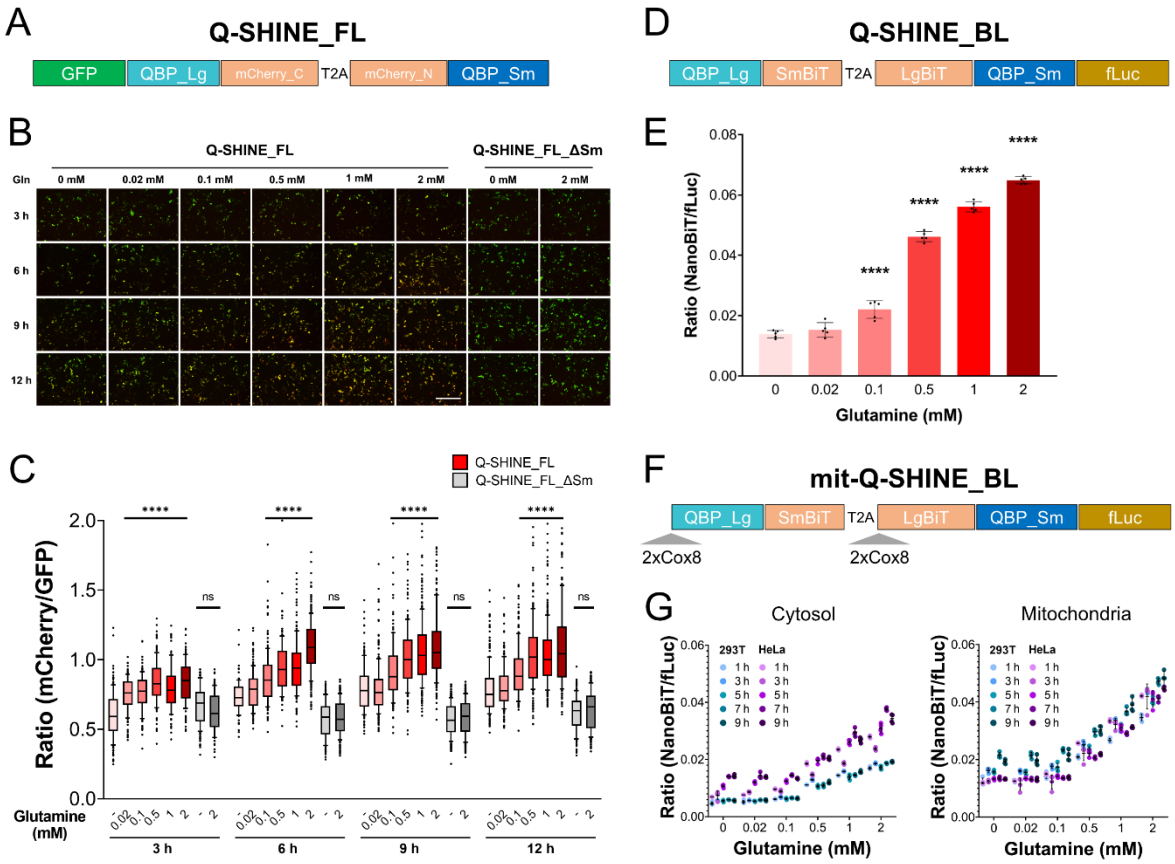
Figure 4. Monitoring Gln changes in living cells. (A) Schematic of the Q-SHINE_FL for the monitoring intracellular Gln level. (B) Fluorescence microscopy of HEK293T cells transfected with Q-SHINE-FL with increasing Gln concentrations. Overlay images from green and red channels are shown. Scale bars, 400 µm. (C) Image-based quantification of mCherry/GFP fluorescence intensity ratio by Q-SHINE_FL at different Gln concentrations. Gln- and time-dependent increase in the fluorescence ratio by Q-SHINE-FL was clearly detected while the ratio of Q-SHINE_FL_ΔSm remained unchanged. The number of ROIs ranges from 89 to 319. The levels of significance are indicated as follows: ****P< 0.0001; n.s., not significant. (D) Schematic of the Q-SHINE_BL for the quantitative analysis of intracellular Gln level. (E) Q-SHINE_BL exhibited highly consistent increase of NanoBiT/fLuc ratio depending on the Gln concentrations. (mean±s.d). (F) mit-Q-SHINE_BL was constructed by addition of 2xCox8 sequences at the N-terminal of final cleaved fragments of Q-SHINE_BL. (G) Bioluminescence ratio in HEK293T and HeLa was compared using Q-SHINE_BL and mit-Q-SHINE_BL by supplementing different Gln concentrations to Gln-starved cells. Error bars represent the s.d. in quadruplicate experiments.